

Maohokite, a post-spinel polymorph of MgFe_2O_4 in shocked gneiss from the Xiuyan crater in China

HPSTAR
716-2019

Ming CHEN ^{1,2*}, Jinfu SHU³, Xiande XIE^{2,4}, and Dayong TAN^{2,4}

¹State Key Laboratory of Isotope Geochemistry, Guangzhou Institute of Geochemistry, Chinese Academy of Sciences, 510640 Guangzhou, China

²Key Laboratory of Mineralogy and Metallogeny, Guangzhou Institute of Geochemistry, Chinese Academy of Sciences, 510640 Guangzhou, China

³Center for High Pressure Science and Technology Advanced Research, 201203 Shanghai, China

⁴Guangdong Provincial Key Laboratory of Mineral Physics and Materials, Guangzhou Institute of Geochemistry, Chinese Academy of Sciences, 510640 Guangzhou, China

*Corresponding author. E-mail: mchen@gig.ac.cn

(Received 02 July 2018; revision accepted 27 October 2018)

Abstract—Maohokite, a post-spinel polymorph of MgFe_2O_4 , was found in shocked gneiss from the Xiuyan crater in China. Maohokite in shocked gneiss coexists with diamond, reidite, $\text{TiO}_2\text{-II}$, as well as diaplectic glasses of quartz and feldspar. Maohokite occurs as nano-sized crystallites. The empirical formula is $(\text{Mg}_{0.62}\text{Fe}_{0.35}\text{Mn}_{0.03})^{2+}\text{Fe}^{3+}_2\text{O}_4$. In situ synchrotron X-ray microdiffraction established maohokite to be orthorhombic with the CaFe_2O_4 -type structure. The cell parameters are $a = 8.907(1) \text{ \AA}$, $b = 9.937(8) \text{ \AA}$, $c = 2.981(1) \text{ \AA}$; $V = 263.8(3) \text{ \AA}^3$; space group *Pnma*. The calculated density of maohokite is 5.33 g cm^{-3} . Maohokite was formed from subsolidus decomposition of ankerite $\text{Ca}(\text{Fe}^{2+}, \text{Mg})(\text{CO}_3)_2$ via a self-oxidation-reduction reaction at impact pressure and temperature of 25–45 GPa and 800–900 °C. The formation of maohokite provides a unique example for decomposition of Fe-Mg carbonate under shock-induced high pressure and high temperature. The mineral and its name have been approved by the Commission on New Minerals, Nomenclature and Classification of the International Mineralogical Association (IMA 2017-047). The mineral was named maohokite after Hokwang Mao, a staff scientist at the Geophysical Laboratory, Carnegie Institution of Washington, for his great contribution to high pressure research.

INTRODUCTION

Ferrous oxide contributes about 8% to the mass of the bulk of Earth's primitive mantle (Lyubetskaya and Korenaga 2007). It was indicated that a significant amount of ferric iron (Fe^{3+}) might exist in the Earth's deep mantle due to the disproportionation reaction of ferrous iron (Fe^{2+}) at high-pressure and high-temperature conditions (Mao 1974; Mao and Bell 1975; Frost et al. 2004; McCammon 2005; Fialin et al. 2009; Rohrbach et al. 2011). Ferrous iron can also be oxidized by other oxidizing agents, such as CO_2 , at mantle pressure–temperature conditions (Boulard et al. 2012). The concentration of ferric iron in the lower mantle should be higher than that in the upper mantle

even though oxygen fugacity decreases with depth (McCammon 2005). The redox state and physical properties of the mantle should have been influenced by the existence of ferric iron in minerals. Then, what would be the most possible carriers of ferric iron in the mantle? The post-spinel phases of MgFe_2O_4 – FeFe_2O_4 were suggested to be the potential host minerals of ferric iron in the lower mantle (Mao et al. 1974; Mao and Bell 1975). Some other high-pressure iron oxides that could occur in the deep Earth, such as HP phases of Fe_2O_3 (Shim et al. 2009; Bykova et al. 2016) and Fe_3O_4 (Fei et al. 1999; Dubrovinsky et al. 2003), as well as HP phases with mixed-valence of Fe_4O_5 (Lavina et al. 2011) and Fe_5O_7 and $\text{Fe}_{25}\text{O}_{32}$ (Bykova et al. 2016) have also been synthesized. Magnesioferrite, MgFe_2O_4 ,

is a Fe^{3+} -rich member of the spinel group, which has been found in kimberlites and carbonatites as well as volcanic fumaroles. The post-spinel transformation in MgFe_2O_4 under high-pressure and high-temperature conditions has been observed experimentally in the laser-heated diamond anvil cell above 20 GPa (Mao and Bell 1975; Andraut and Bolfan-Casanova 2001; Winell et al. 2006). However, no post-spinel phase of MgFe_2O_4 has been previously found in nature.

The deep mantle contains abundant high-pressure minerals but most of them cannot be preserved during the long journey to the surface. The naturally impacted terrestrial rocks or meteorites provide the major sources of high-pressure minerals that may predominate in the Earth's deep mantle. A lot of high-pressure minerals that may predominate in the deep mantle, such as coesite and stishovite (Chao et al. 1962), ringwoodite (Binns et al. 1969), bridgmanite (Tschauner et al. 2014) and others, have been found in naturally impacted terrestrial rocks and meteorites, which provide a window to look into the mineral constituents of the mantle rocks (e.g., Stöffler 1997; Akaogi 2000).

The Xiuyan crater is a bowl-shaped structure 1.8 km in diameter of where the crystalline rocks are composed of the Early Proterozoic gneiss-amphibolite-marble complexes. This crater was confirmed as a meteorite impact site through the discovery of a series of shock-metamorphic features of minerals in impacted rocks (Chen et al. 2010a, 2010b, 2011, 2013a, 2013b). In a study of shocked ankerite from impact breccia of the crater, we discovered a shock-induced post-spinel polymorph of MgFe_2O_4 . This mineral and its name have been approved by the Commission on New Minerals, Nomenclature and Classification of the International Mineralogical Association (IMA 2017-047). The mineral has been named maohokite after Hokwang Mao of the Geophysical Laboratory, Carnegie Institution of Washington, in honor of his great contribution to high-pressure research.

SAMPLES AND METHODS

The investigated samples of impact breccia were collected from the drill cores into the depth interval of 260–295 m at the center of the Xiuyan crater. The impact breccias are composed of fragments of gneiss, amphibolite, marble, and fine-grained matrix.

Gneiss fragments picked up from the impact breccias were cut into slices and then polished into 30 μm thick for phase identifications. The bulk compositions of shocked ankerite in gneiss were analyzed by a JEOL JXA-8100 electron microprobe with the wavelength dispersive technique at 15 kV accelerating voltage and 10 nA beam current. Raman

spectra of shocked ankerite were recorded with a Renishaw R-2000 instrument. A microscope was used to focus the excitation beams (514.5 nm and 638 nm lasers) to 1 μm wide spots and to collect the Raman signal.

X-ray diffraction analyses of shocked ankerite were conducted in situ on the polished thin sections of gneiss by synchrotron X-ray microdiffraction analysis on the Beamline 12.3.2 at the Advance Light Source of the Lawrence Berkeley National Laboratory, USA. The X-ray energy was 10.0001 KeV ($\lambda = 1.23986 \text{ \AA}$). The synchrotron X-ray microdiffraction analysis with a beam size of $<1 \mu\text{m}$ was used to scan the sample spot by spot, to obtain diffraction signals. The diffraction patterns were collected with aMAR133CCD detector at a distance of 137.714 mm from the sample. The experimental setup was calibrated by an Alumina standard, Al_2O_3 . The data collection time for each pattern was kept unchanged as 300 s through the whole experiment. The diffraction data were processed by using the program XMAS V.6 (IDL Virtual Machine, X-ray diffraction analysis software).

In preparation for the study with STEM and TEM, flakes of shocked ankerite were extracted by the focused ion beam (FIB) milling technique with a FEI Versa 3D Dual Beam FIB/SEM system at the Center for High Pressure Science and Technology Advanced Research, Shanghai, China. The samples were thinned to $10 \times 5 \mu\text{m}$ flakes with a thickness of 90 nm by using a Ga^+ FIB operating at 30 kV and currents from 0.5 nA down to 48 pA for final surfacing. The phase identifications were performed with a FEI Talos F200s scanning/transmission electron microscope operating at 200 kV, equipped with a field emission gun, at Guangzhou Institute of Geochemistry, Chinese Academy of Sciences, China. Bright-field, high-resolution bright-field, and STEM images of minerals as well as selected area electron diffractions in TEM were obtained from the samples. Compositional analysis of nano-sized crystallites of maohokite and magnesioferrite was conducted by using EDXS with an accelerating voltage of 200 kV, a beam current of 1 nA, and a beam size of $\sim 5 \text{ nm}$ in STEM mode. Accumulation time of X-ray signals was 5 s per analysis.

RESULTS

Occurrence

The investigated gneiss from impact breccia of the Xiuyan crater is composed of about 55 vol% feldspar, 38 vol% quartz, and 5 vol% ankerite (Fig. 1a). We have identified three kinds of gneiss fragments according to shock-metamorphic features, i.e., slightly,

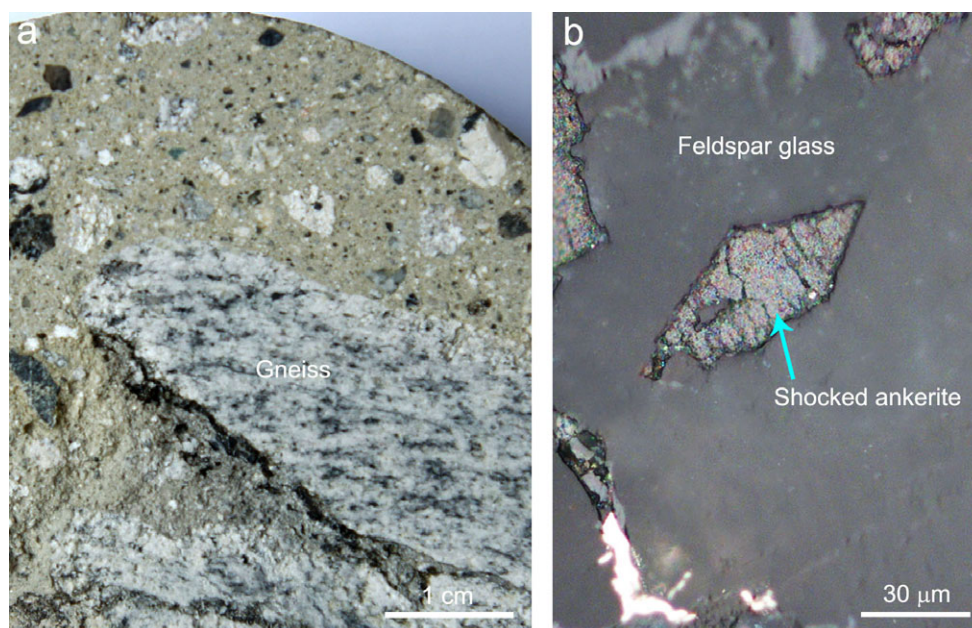


Fig. 1. Polymict impact breccias from the drill cores in the Xiuyan crater. a) Gneiss fragments in the impact breccia. b) Shocked ankerite enclosed in feldspar glass within gneiss, plane-polarized reflected light. (Color figure can be viewed at wileyonlinelibrary.com.)

moderately, and strongly shocked gneisses. In the slightly shocked gneiss, most of the minerals remain intact or display some planar deformation features in quartz and feldspars (Chen et al. 2011). The strongly shocked gneiss was shock-melted and contains abundant coesite that had crystallized from shock-induced silica melt (Chen et al. 2010b). The moderately shocked gneiss is characterized by extensive solid-state phase transformation of minerals. Quartz has been completely transformed into diaplectic glass that has retained the previous morphological character of a quartz crystal, and feldspar partially transformed into diaplectic glass. Accessory minerals of rutile and zircon have been partially transformed into high-pressure polymorph of TiO_2 -II (Chen et al. 2013a) and reidite (Chen et al. 2013b), respectively. About 30% of the rutile in the gneiss transformed to TiO_2 -II. Maohokite occurs in the moderately shocked gneiss.

Most grains of ankerite in the moderately shocked gneiss still preserve their original crystal morphologies (Fig. 1b), but are now decomposed into a multiphase mixture composed of magnesioferrite, maohokite, calcite, and diamond (Fig. 2a) (Chen et al. 2018). Electron microprobe analyses of shocked ankerite show a bulk composition of $\text{Ca}(\text{Fe}_{0.59}\text{Mg}_{0.33}\text{Ca}_{0.07}\text{Mn}_{0.01})(\text{CO}_3)_2$. Magnesioferrite occurs as crystallites up to 200 nm in size (Fig. 2a). Maohokite occurs as crystallites 2–30 nm in size (Figs. 2a and 2d). The contents of maohokite and magnesioferrite in the

shocked ankerite are about 8% and about 20%, respectively. The crystal size of diamond varies from 2 to 5 nm (Chen et al. 2018). Calcite occurs as crystallite aggregates with individual crystal size ranging from 5 to 300 nm. Some irregular bubbles up to 150 nm in size can be observed within the shocked ankerite.

Chemical Composition and Crystallography

The energy dispersive X-ray microanalyses of nano-sized crystallites of maohokite and magnesioferrite clearly indicate the compositions of magnesium-iron oxides (Fig. 2b). The compositional analyses show that maohokite has the same composition as magnesioferrite, and contains 75.12 (73.62–76.02) wt% Fe_2O_3 , 11.95 (8.74–13.05) wt% MgO , 11.93 (9.92–16.25) wt% FeO , and 1.00 (0.67–1.34) wt% MnO . The empirical formula of maohokite is $(\text{Mg}_{0.62}\text{Fe}_{0.35}\text{Mn}_{0.03})^{2+}\text{Fe}^{3+}_2\text{O}_4$. The simplified formula of maohokite is MgFe_2O_4 . The composition of magnesioferrite in our samples is close to 2:1 solid solution of magnesioferrite : magnetite.

Synchrotron-based micro-X-ray diffraction analyses were carried out to determine the crystalline phases present in the shocked ankerite. Four different phases including maohokite, magnesioferrite, calcite, and diamond have been identified (Chen et al. 2018). Figure 3 is an X-ray diffraction pattern from which 23 diffraction lines can be assigned to maohokite, and indexed to an orthorhombic CaFe_2O_4 -type structure with space group $Pnma$ (Table 1).

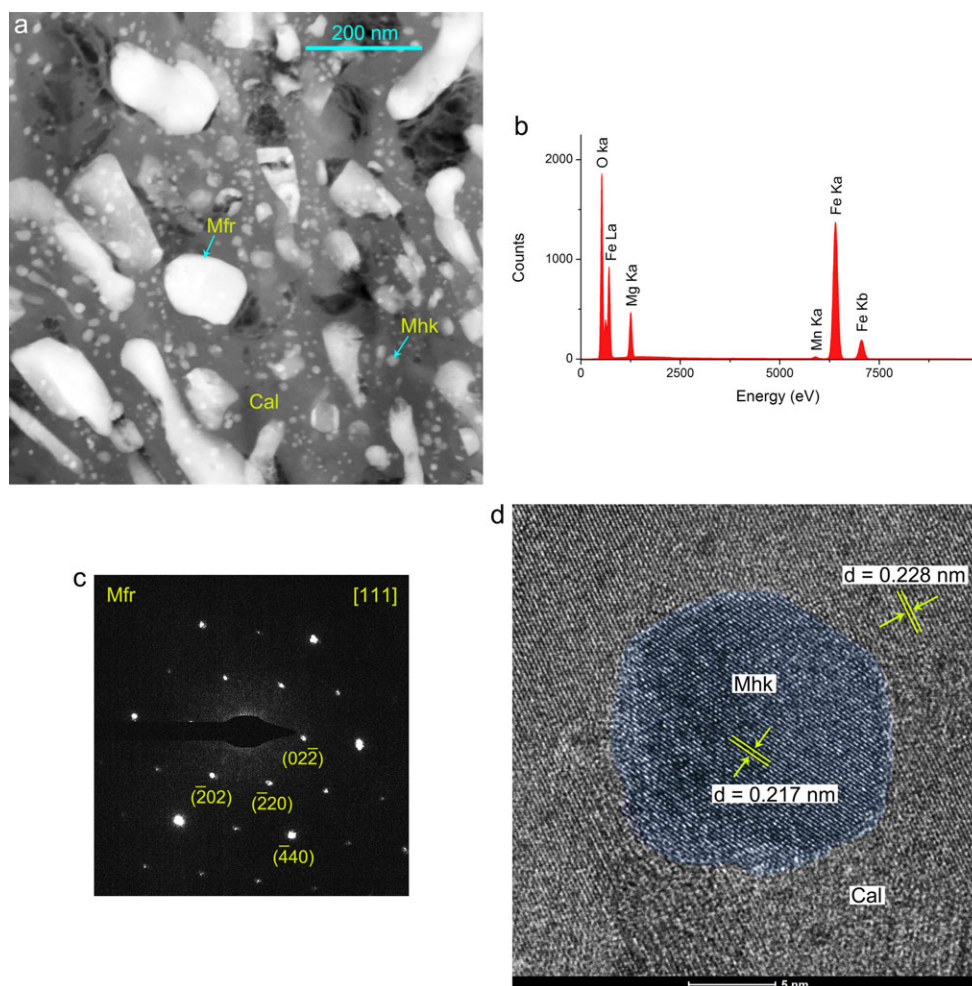


Fig. 2. Maohokite in shocked ankerite. a) A STEM image of shocked ankerite shows tiny crystallites of maohokite (Mhk) and magnesioferrite (Mfr) embedded in calcite (Cal). b) An EDS spectrum of maohokite (or magnesioferrite) shows three major elements including oxygen, iron, and magnesium as well as the minor element manganese. c) A selected area electron diffraction (SAED) pattern of magnesioferrite (Mfr) corresponding to the [111] zone axis. d) A high-resolution image showing a maohokite crystal with the lattice fringes of 0.217 nm corresponding to the {410} planes. Calcite surrounding this maohokite crystal displays the lattice fringes of 0.228 nm corresponding to the {113} planes. (Color figure can be viewed at wileyonlinelibrary.com.)

The cell parameters of maohokite are: $a = 8.907(1) \text{ \AA}$, $b = 9.937(8) \text{ \AA}$, $c = 2.981(1) \text{ \AA}$, $V = 263.8(3) \text{ \AA}^3$. The calculated density of maohokite is 5.33 g cm^{-3} . The density of magnesioferrite is $4.6\text{--}4.7 \text{ g cm}^{-3}$. Greater density of maohokite than magnesioferrite demonstrates that maohokite is a high-pressure polymorph of magnesioferrite.

The nanocrystallites of maohokite and magnesioferrite have been further characterized by transmission electron microscopy (TEM) and electron diffraction analysis. Figure 2c displays an electron diffraction pattern of the [111] zone axis of magnesioferrite. The lattice fringes of maohokite with spacings of 0.266, 0.248, 0.245, and 0.217 nm, which can be indexed to the {230}, {201}, {121}, and {410} planes, respectively, have been observed by high-resolution TEM (Fig. 2d).

Raman Spectroscopy

The crystalline phases in shocked ankerite have been characterized by Raman spectroscopy (Fig. 4). The strong band at 1086 cm^{-1} and weak band at 279 cm^{-1} can be assigned to calcite (Sun et al. 2014). The strong band at 686 cm^{-1} and some weak bands at 554, 478, 328, and 210 cm^{-1} are attributed to magnesioferrite (Winell et al. 2006), and the strong band at 602 cm^{-1} to maohokite, in comparison to the Raman spectrum of post-spinel polymorph of FeCr_2O_4 (Chen et al. 2003). Raman spectra of both magnesioferrite and magnetite usually display a strong and well-defined A_{1g} band at approximately 670 cm^{-1} and 700 cm^{-1} , respectively (D'Ippolito et al. 2015). The observed strong band of magnesioferrite at 686 cm^{-1} for our sample, which falls in between 670 cm^{-1}

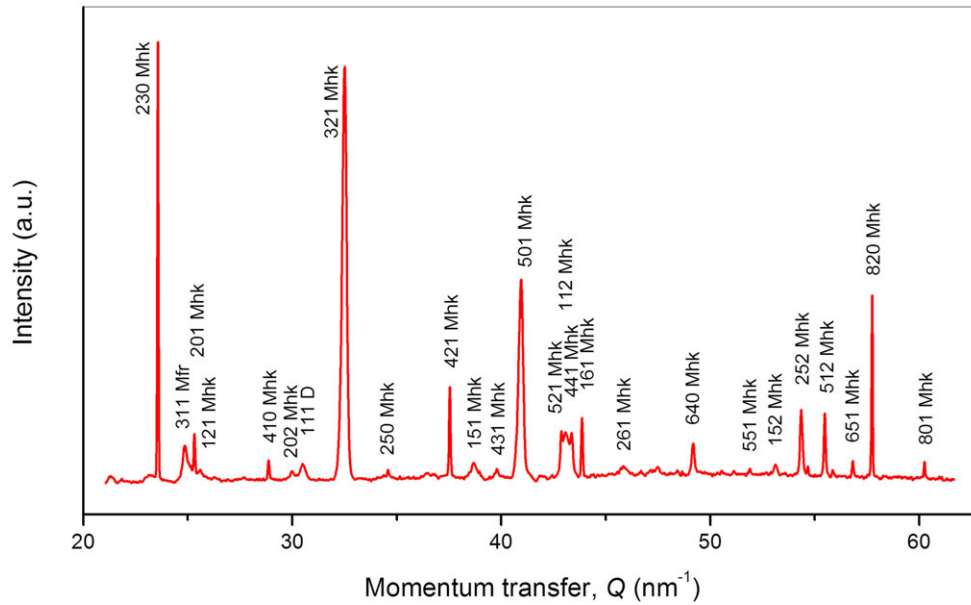


Fig. 3. X-ray diffraction pattern mainly indexed to maohokite (Mhk), in which two weak lines are assigned to magnesioferrite (Mfr) and diamond (D), respectively. (Color figure can be viewed at wileyonlinelibrary.com.)

Table 1. Peak assignment and Miller indices for the X-ray diffraction pattern of maohokite.

I_{obs} (%)	d_{obs} (Å)	d_{calc} (Å)	d_{diff} (Å)	hkl
100	2.663	2.658	0.005	2 3 0
10	2.481	2.477	0.004	2 0 1
4	2.455	2.457	-0.002	1 2 1
6	2.175	2.173	0.002	4 1 0
90	1.932	1.937	-0.005	3 2 1
4	1.816	1.815	0.001	2 5 0
20	1.673	1.679	-0.006	4 2 1
7	1.624	1.626	-0.002	1 5 1
4	1.578	1.571	0.007	4 3 1
50	1.533	1.529	0.004	5 0 1
10	1.465	1.462	0.003	5 2 1
10	1.457	1.454	0.003	1 1 2
10	1.448	1.449	-0.001	4 4 1
12	1.431	1.429	0.002	1 6 1
5	1.371	1.377	-0.006	2 6 1
8	1.276	1.274	0.002	6 4 0
2	1.210	1.212	-0.002	5 5 1
4	1.183	1.182	0.001	1 5 2
15	1.155	1.152	0.003	2 5 2
12	1.131	1.136	-0.004	5 1 2
5	1.105	1.105	0.000	6 5 1
30	1.087	1.087	0.000	8 2 0
5	1.042	1.043	-0.001	8 0 1

d_{obs} = observed d spacing; d_{calc} = d spacing calculated with measured cell parameters; d_{diff} = difference between d_{obs} and d_{calc} ; hkl = Miller indices.

(magnetite) and 700 cm^{-1} (magnesioferrite), is in agreement with the composition of magnesioferrite close to 2:1 solid solution of magnesioferrite : magnetite.

DISCUSSION

According to the shock-metamorphic features of minerals in the moderately shocked gneiss in the Xiuyan impact breccia, we estimate the pressure and temperature conditions for the formation of maohokite. The transformation of quartz and feldspar to diaplectic glasses constrains shock pressure and temperature to 35–45 GPa and 300–900 °C (Grieve et al. 1996). The moderately shocked gneiss contains abundant $\text{TiO}_2\text{-II}$ phase transformed from rutile. The transformation of rutile to $\text{TiO}_2\text{-II}$ can be produced by high-pressure shock-loading above 20 GPa (McQueen et al. 1967), and the highest yield of $\text{TiO}_2\text{-II}$ was achieved at a peak pressure of ~45 GPa (Kusaba et al. 1988). However, the transition from rutile to $\text{TiO}_2\text{-II}$ is sluggish at temperature below 800 °C (Akaogi et al. 1992). Laboratory experiments revealed that magnesioferrite transforms to a high-pressure form at 20 GPa after laser heating (Mao and Bell 1975). The spinel/post-spinel transition boundaries for the endmembers of magnesioferrite at 25 GPa (Andraut and Bolfan-Casanova 2001) and magnetite at 23.6 GPa (Fei et al. 1999) are within the above shock P – T constraints. Therefore, we suggest that maohokite crystallized at 25–45 GPa and 800–900 °C.

The decomposition of ankerite corresponds to a subsolidus self-redox reaction of $6\text{Ca}(\text{Fe,Mg})(\text{CO}_3)_2 \rightarrow 6\text{CaCO}_3 + 2\text{MgFe}_2\text{O}_4 + \text{C} + 5\text{CO}_2$ at high pressure and high temperature (Chen et al. 2018). In this reaction, part of the Fe^{2+} of ankerite was oxidized to Fe^{3+} by concurrent reduction of part of the C^{4+} to

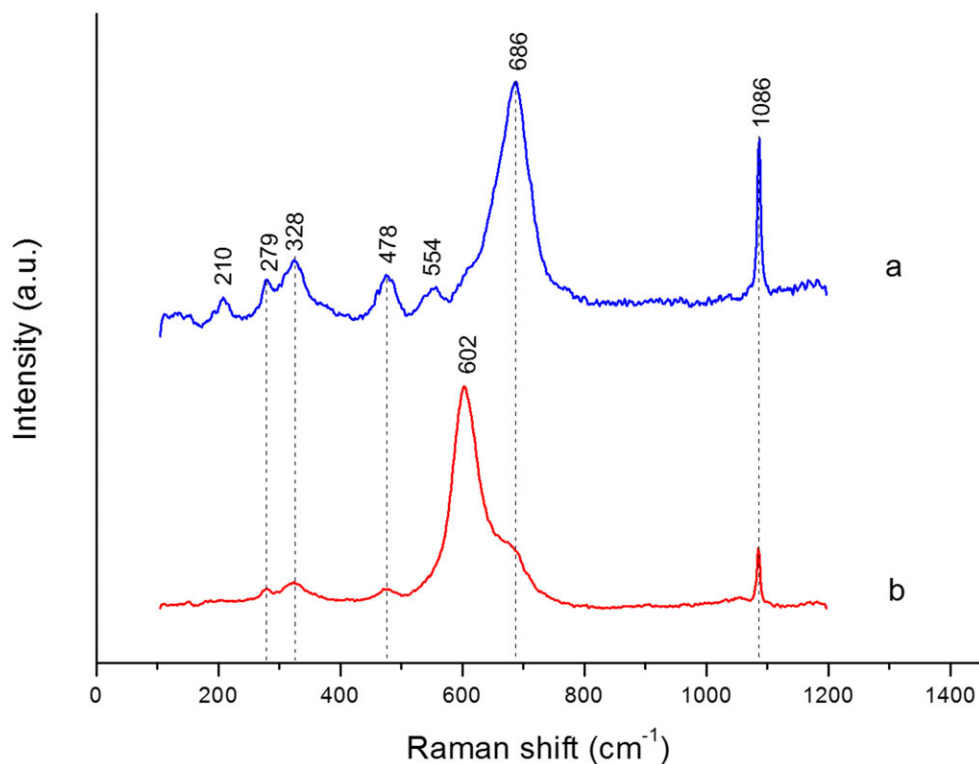


Fig. 4. Raman spectra of shocked ankerite collected with the 514 nm laser. The bands at 686, 554, 478, and 328 cm^{-1} are attributed to magnesioferrite, whereas the strong band at 602 cm^{-1} corresponds to maohokite. The strong band at 1086 cm^{-1} and the weak band at 279 cm^{-1} are assigned to calcite. The spectrum (a) characterizes two major phases of magnesioferrite plus calcite, whereas the spectrum (b) characterizes two major phases of maohokite plus calcite and minor magnesioferrite. (Color figure can be viewed at wileyonlinelibrary.com.)

C^0 . The Fe_2O_3 and MgO decomposed from ankerite combine together to form maohokite or magnesioferrite. The pressure pulse triggered by a meteorite (or asteroid) impact is a transient process, only milliseconds or seconds for large-scale collisions (Stöffler et al. 1991). The coexistence of maohokite and magnesioferrite in the samples indicates a rapid change in pressure over a relatively short time. Maohokite crystallized in the high-pressure regime only occurs as tiny nanocrystallites, whereas magnesioferrite crystallized after pressure release has relatively large sizes of crystallites.

The decomposition of Fe-rich carbonates has also been observed in terrestrial metamorphic rocks (Zuilen et al. 2003), high-pressure/high-temperature experiments (Tao et al. 2013; Kang et al. 2015), in shock-metamorphosed meteorites (Brearley 2003), and in shock experiments (Bell 2007), respectively. The decomposition of Fe-rich carbonates usually involves an oxidation–reduction reaction resulting in the conversion of Fe^{2+} to Fe^{3+} and C^{4+} to C^0 (Brearley 2003; Zuilen et al. 2003; Bell 2007; Kang et al. 2015). The decomposition of Fe-rich carbonates leads to the formation of magnetite and graphite, and has been generally attributed to a thermal effect (Brearley 2003; Zuilen et al. 2003; Bell 2007). The

formation of maohokite provides a unique example for decomposition of Fe–Mg carbonate under shock-induced high pressure and high temperature.

The crystal structures related to the tunnel structures of CaFe_2O_4 (CF), CaTi_2O_4 (CT), and CaMn_2O_4 (CM) are considered as post-spinel phases (Irifune et al. 1991; Kirby et al. 1996; Galuskin et al. 2016). So far, only three ferric iron oxide minerals with post-spinel structures, which include maohokite (CF) in this study, $\text{CaFe}^{3+}_2\text{O}_4$ harmunite (CF) (Galuskina et al. 2014) and $\text{CaFe}^{3+}_2\text{Mn}^{4+}\text{O}_4$ wernerkrauseite (CF) (Galuskin et al. 2016), have been identified in nature. Maohokite is a high-pressure mineral that can be stable at lower mantle conditions. Harmunite and wernerkrauseite were formed in pyrometamorphic rocks of a volcano and belong to the group of low-pressure minerals. The natural occurrence of maohokite puts it into the category of potential mantle minerals and provides significant insights into the host phase of ferric iron in the lower mantle.

Magnesiowüstite (Mg,Fe)O is believed to be an important constituent of the lower mantle (Zhang and Herzberg 1994; Agee et al. 1995). A previous investigation of $(\text{Mg}_{0.35}\text{Fe}_{0.65})\text{O}$ inclusions in diamond

from kimberlite reported the finding of magnesioferrite nanocrystallites that is embedded in a magnesiowüstite matrix, and the formation of magnesioferrite is attributed to the reversion from its high-pressure polymorph (Wirth et al. 2014). Fe^{3+} -rich clusters ($\text{Mg}_{1+x}\text{Fe}_{2-x}\text{O}_{4-x/2}$) have been also identified from magnesiowüstite inclusions in kimberlitic lower mantle diamonds (Kaminsky et al. 2015). The natural occurrence of Fe^{3+} -rich ferromagnesian oxides from mantle rocks gives evidence for the existence of ferric iron in the Earth's deep interior. If a significant amount of ferrous iron in the deep mantle would have been converted to ferric iron via chemical reactions at high temperature and high pressure, maohokite might behave as an important carrier of ferric iron in the ferromagnesian mantle.

High-pressure mineral evidence for shock-induced high-pressure phase transformation of carbonates has so far never been found in terrestrial impact rocks and shock-metamorphic meteorites. The finding of maohokite and diamond (Chen et al. 2018) decomposed from ferromagnesian carbonate in the Xiuyan crater provides new evidence on the shock effects of high pressure and high temperature in carbonate.

Acknowledgments—The authors are grateful to two anonymous reviewers and the Associate Editor W. U. Reimold for their constructive comments that helped improve the manuscript. We thank Y. P. Yang from HPSTAR in Shanghai for FIB milling of TEM samples; H. Y. Xian from GIGCAS in Guangzhou for the assistance of STEM and TEM analyses; and B. B. Yue (HPSTAR), F. Hong (HPSTAR), and N. Tamura (ALS) of Beamline 12.3.2 at the Advanced Light Source of the Lawrence Berkeley National Laboratory for help with the synchrotron X-ray diffraction analysis. This work is supported by the Strategic Priority Research Program (B) of the Chinese Academy of Sciences (XDB18010405) and the National Natural Science Foundation of China (41672032).

Editorial Handling—Dr. W. Uwe Reimold

REFERENCES

- Agee C., Li J., Shannon M. C., and Circone S. 1995. Pressure-temperature phase diagram for the Allende meteorite. *Journal of Geophysical Research* 100:17,725–17,740.
- Akaogi M. 2000. Clues from a shocked meteorite. *Science* 287:1602–1603.
- Akaogi M., Kusaba K., Susaki J., Yagi T., Matsui M., Kikegawa T., Yusa H., and Ito E. 1992. High-pressure high-temperature stability of α - PbO_2 -type TiO_2 and MgSiO_3 majorite: Calorimetric and in situ X-ray diffraction studies. In *High-pressure research: Application to earth and planetary sciences*, edited by Syono Y. and Manghnani M. H. Washington, D.C.: American Geophysical Union. pp. 447–455.
- Andraut D. and Bolfan-Casanova N. 2001. High-pressure phase transformations in the MgFe_2O_4 and Fe_2O_3 - MgSiO_3 systems. *Physics and Chemistry of Minerals* 28:211–217.
- Bell M. S. 2007. Experimental shock decomposition of siderite and the origin of magnetite in Martian meteorite ALH 84001. *Meteoritics & Planetary Science* 42:935–949.
- Binns R. A., Davis R. J., and Reed S. J. B. 1969. Ringwoodite, natural $(\text{Mg}, \text{Fe})_2\text{SiO}_4$ spinel group in the Tenham meteorite. *Nature* 221:943–944.
- Boulard E., Menguy N., Auzende A. L., Benzerara K., Bureau H., Antonangeli D., Corgne A., Morard G., Siebert J., Perrillat J. P., Guyot F., and Fiquet G. 2012. Experimental investigation of the stability of Fe-rich carbonates in the lower mantle. *Journal of Geophysical Research* 117:B02208.
- Brearley A. J. 2003. Magnetite in ALH 84001: An origin by shock induced thermal decomposition of iron carbonate. *Meteoritics & Planetary Science* 38:849–870.
- Bykova E., Dubrovinsky L., Dubrovinskaia N., Bykov M., McCammon C., Ovsyannikov S. V., Liermann H. P., Kuppenko I., Chumakov A. I., Rüffer R., Hanfland M., and Prakapenka V. 2016. Structural complexity of simple Fe_2O_3 at high pressures and temperatures. *Nature Communications* 7:10,661.
- Chao E. C. T., Fahey J. J., Littler J., and Milton E. J. 1962. Stishovite, a very high pressure new mineral from Meteor Crater, AZ. *Journal of Geophysical Research* 67:419–421.
- Chen M., Shu J. F., Xie X., and Mao H. K. 2003. Natural CaTi_2O_4 -structured FeCr_2O_4 polymorph in the Suizhou meteorite and its significance in mantle mineralogy. *Geochimica et Cosmochimica Acta* 67:3937–3942.
- Chen M., Xiao W., Xie X., Tan D., and Cao Y. 2010a. Xiuyan crater, China: Impact origin confirmed. *Chinese Science Bulletin* 55:1777–1781.
- Chen M., Xiao W., and Xie X. 2010b. Coesite and quartz characteristic of crystallization from shock-produced silica melt in the Xiuyan crater. *Earth and Planetary Science Letters* 297:306–314.
- Chen M., Koeberl C., Xiao W., Xie X., and Tan D. 2011. Planar deformation features in quartz from impact-produced polymict breccia of the Xiuyan crater, China. *Meteoritics & Planetary Science* 46:729–736.
- Chen M., Gu X., Xie X., and Yin F. 2013a. High-pressure polymorph of TiO_2 -II from the Xiuyan crater of China. *Chinese Science Bulletin* 58:4655–4662.
- Chen M., Feng Y., Li X., Xie X., Xiao W., and Tan D. 2013b. Natural occurrence of reidite in the Xiuyan crater of China. *Meteoritics & Planetary Science* 48:796–805.
- Chen M., Shu J., Xie X., Tan D., and Mao H. K. 2018. Natural diamond formation by self-redox of ferromagnesian carbonate. *Proceedings of the National Academy of Sciences* 115:2676–2680.
- D'Ippolito V., Andreozzi G. B., Bersani D., and Lottici P. P. 2015. Raman fingerprint of chromate, aluminate and ferrite spinels. *Journal of Raman Spectroscopy* 46:1255–1264.
- Dubrovinsky L. S., Dubrovinskaia N. A., McCammon C., Rozenberg G. K., Ahuja R., Osorio-Guillen J. M., Dmitriev V., Webe H.-P., Le Bihan T., and Johansson B. 2003. The structure of the metallic high-pressure Fe_3O_4

- polymorph: Experimental and theoretical study. *Journal of Physics-Condensed Matter* 15:7697–7706.
- Fei Y., Frost D. J., Mao H. K., Prewitt C. T., and Häusermann D. 1999. In situ structure determination of the high-pressure phase of Fe_3O_4 . *American Mineralogist* 84:203–206.
- Fialin M., Catillon G., and Andraut D. 2009. Disproportionation of Fe^{2+} in Al-free silicate perovskite in the laser heated diamond anvil cell as recorded by electron probe microanalysis of oxygen. *Physics and Chemistry of Minerals* 36:183–191.
- Frost D. J., Liebske C., Langenhorst F., McCammon C. A., Trønnes R. G., and Rubie D. C. 2004. Experimental evidence for the existence of iron-rich metal in the Earth's lower mantle. *Nature* 428:409–412.
- Galuskin E. V., Krüger B., Krüger H., Blass G., Widmer R., and Galuskin I. O. 2016. Wernerkrauseite, $\text{CaFe}^{3+}_2\text{Mn}^{4+}\text{O}_6$ —The first non-stoichiometric postspinel mineral, from Bellerberg volcano, Eifel, Germany. *European Journal of Mineralogy* 28:485–493.
- Galuskin I., Vapnik Y., Lazic B., Armbruster T., Murashko M., and Galuskin E. 2014. Harmunite, CaFe_2O_4 —a new mineral from the Jabel Harmun, West Bank, Palestinian Autonomy, Israel. *American Mineralogist* 99:965–975.
- Grieve R. A. F., Langenhorst F., and Stöffler D. 1996. Shock metamorphism of quartz in nature and experiment: II. Significance in geoscience. *Meteoritics & Planetary Science* 31:6–35.
- Irifune T., Fujino K., and Ohtani K. 1991. A new high pressure form of MgAl_2O_4 . *Nature* 349:409–411.
- Kaminsky F. V., Ryabchikov I. D., McCammon C. A., Longo M., Abakumov A. M., Turner S., and Heidari H. 2015. Oxidation potential in the Earth's lower mantle as recorded by ferroprecipitate inclusions in diamond. *Earth and Planetary Science Letters* 417:49–56.
- Kang N., Schmidt M. W., Poli S., Franzolin E., and Connolly J. A. D. 2015. Melting of siderite to 20 GPa and thermodynamic properties of FeCO_3 -melt. *Chemical Geology* 400:34–43.
- Kirby S. H., Stein S., Okai E. A., and Rubie D. C. 1996. Metastable mantle phase transformations and deep earthquakes in subducting oceanic lithosphere. *Reviews of Geophysics* 34:261–306.
- Kusaba K., Kikuchi M., Fukuoka K., and Syono Y. 1988. Anisotropic phase transition of rutile under shock compression. *Physics and Chemistry of Minerals* 15:238–245.
- Lavina B., Dera P., Kim E., Meng Y., Downse R. T., Weck P. F., Sutton S. R., and Zhao Y. 2011. Discovery of the recoverable high-pressure iron oxide Fe_4O_5 . *Proceedings of the National Academy of Sciences* 108:17,281–18,285.
- Lyubetskaya T. and Korenaga J. 2007. Chemical composition of Earth's primitive mantle and its variance: 1. Method and results. *Journal of Geophysical Research* 112:B03211.
- Mao H. K. 1974. A discussion of the iron oxides at high pressure with implications for the chemical and thermal evolution of the Earth. *Carnegie Institution of Washington Year Book* 73:510–518.
- Mao H. K. and Bell P. M. 1975. High-pressure transformation in magnesioferrite (MgFe_2O_4). *Carnegie Institution of Washington Year Book* 75:555–557.
- Mao H. K., Takahashi T., Bassett W. A., Kinsland G. L., and Merrill L. 1974. Isothermal compression of magnetite to 320 Kbar and pressure-induced phase transformation. *Journal of Geophysical Research* 79:1165–1170.
- McCammon C. 2005. The paradox of mantle redox. *Science* 308:807–808.
- McQueen R. G., Jamieson J. C., and Marsh S. P. 1967. Shock-wave compression and X-ray studies of titanium dioxide. *Science* 155:1401–1404.
- Rohrbach A., Ballhaus C., Ulmer P., Golla-Schindler U., and Schönbohm D. 2011. Experimental evidence for a reduced metal-saturated upper mantle. *Journal of Petrology* 52:717–731.
- Shim S. H., Bengtson A., Morgan D., Sturhahn W., Catalli K., Zhao J., Lerche M., and Prakapenka V. 2009. Electronic and magnetic structures of the postperovskite-type Fe_2O_3 and implications for planetary magnetic records and deep interiors. *Proceedings of the National Academy of Sciences* 106:5508–5512.
- Stöffler D. 1997. Minerals in the deep Earth: A message from the asteroid belt. *Science* 278:1576–1577.
- Stöffler D., Keil K., and Scott E. R. D. 1991. Shock metamorphism of ordinary chondrites. *Geochimica et Cosmochimica Acta* 55:3845–3867.
- Sun J., Wu Z., Cheng H., Zhang Z., and Frost R. L. 2014. A Raman spectroscopic comparison of calcite and dolomite. *Spectrochimica Acta A* 117:158–162.
- Tao R., Fei Y. W., and Zhang L. F. 2013. Experimental determination of siderite stability at high pressure. *American Mineralogist* 98:1565–1572.
- Tschauner O., Ma C., Beckett J. R., Prescher C., Prakapenka V. B., and Rossman G. R. 2014. Discovery of bridgmanite, the most abundant mineral in Earth, in a shocked meteorite. *Science* 346:1100–1102.
- Winell S., Annersten H., and Prakapenka V. 2006. The high-pressure phase transformation and breakdown of MgFe_2O_4 . *American Mineralogist* 91:560–567.
- Wirth R., Dobrzhinetskaya L., Harte B., Schreiber A., and Green H. W. 2014. High-Fe (Mg, Fe)O inclusion in diamond apparently from the lowermost mantle. *Earth and Planetary Science Letters* 404:365–375.
- Zhang J. and Herzberg C. 1994. Melting experiments on anhydrous peridotite KLB-1 from 5.0 to 22.5 GPa. *Journal of Geophysical Research* 99:17,729–17,742.
- Zuilen M. A., Lepland A., Teranes J., Finarelli J., Wahlen M., and Arrhenius G. 2003. Graphite and carbonates in the 3.8 Ga old Isua Supracrustal Belt, southern West Greenland. *Precambrian Research* 126:331–348.